An analysis of heat source/sink influence on MHD fluid flow past a vertically enhanced plate with radiations

DOI : 10.36909/jer.17737

Shipra*

Department of Applied Sciences, Punjabi University COEM, Rampuraphul

* Corresponding Author: shipracoem@pbi.ac.in

ABSTRACT

This paper explores the heat source/sink influence on irregular flow across a uniformly moving stretch sheet with of magnetic field. Flow equations are tackled with Laplace transformation technique. Tables and graphs drawn with MATLAB software show the effects of various physical parameters discovered during the numerical simulation on velocity, temperature, concentration, heat and mass transfer rate. The temperature is demonstrated to be reduced by the radiation and heat absorption parameters. Results reveal that concentration improves with enhancement of time. Furthermore, fluid velocity reduces with enhancement in viscosity. Solar energy collection systems, geophysics, astrophysics, aerospace and the design of high temperature manufacturing process systems are all examples of where the model can be used. The consistency of the model predictions is determined by comparing the findings to previously published literature. The article is unique and fills the gap in literature that the combined effects of heat source/sink with radiations and magnetism have rarely been researched.

Keywords: Magnetohydrodynamics, Radiation, Heat Source/Sink, Free Convection.

INTRODUCTION

MHD free convection flow research offers a wide range of applications in varied fields. Several writers have contributed to the solution of issues involving free convective flows in varied boundary environments. Slanting magnetic field effects on a spontaneously started infinite perpendicular isothermal plate with fluctuating temperature and an electrically conductive fluid moving over it were studied by (Soundalgekar et al., 1981). (Rajput and Sahu, 2011) investigated natural circulation flow among two vertically unbounded parallel surfaces with fixed heat. (England and Emery, 1969) examined the radiative heat effects surrounding a visibly thin grey gas confined by a fixed vertical plate. The radiative effects on variable viscosity across an impermeable flat channel was studied by (Hossain and Takhar, 1996). The radiative effects on flow through an infinitely uniform flat channel were investigated by (Das et al., 1996). Recently, (Garg et al., 2015) looked into the turbulent free convective flow in a vertical route across a flexible material at defined thermal radiation bounds. (Kandasamy et al., 2010) used a vertical stretching layer to investigate the effects of mass and heat transport, along with chemical changes and MHD flow. (Garg and Shipra, 2019) looked into heat source/sink effects on flow through a flat channel that started impulsively with varied heat transfer rate. (Basant and Gabriel, 2020) examined heat source/sink effects on MHD free convective flow in a channel filled with nanofluid. Latest research in this field can be seen in work of (Abdelrazik et al., 2020; Kumar et al., 2020; Wakif et al., 2020; Afzal et al., 2021).

Motivated by above ref. works, present study explores heat source/sink influence with thermal radiations on irregular free-convective flow over a radially accelerated flat channel. To the best of author's perspective, the combined heat source/sink influence with thermal radiations have been ignored in most of studies. The paper is closely related to work of (Garg et al., 2011).The novelty of this article over (Garg et al., 2011) is inclusion of heat source /sink parameter in energy equation. The impact of the prominent parameters on velocity, temperature, concentration, the rate of heat and mass

transfer have been represented using graphs and tables. Symbolic software MATLAB has been used to draw various graphs. Complementary error and exponential functions are used to illustrate the results.

MATHEMATICAL ANALYSIS

The flow of an incompressible, electrically conducting radiated fluid through a vertical plate that's been linearly accelerated, is considered. Y'-axis is upright to the x'-axis, which is perpendicularly up. Fluid and plate are first kept in a stationary state at the same temperature. Plate is accelerated with $u = u_o t'$ at $t' > 0$. The concentration and temperature of the plate have been boosted slightly to $C_w{}'$ and $T_w{}'$. With above conditions, the flow field is governed as:

$$\frac{\partial u'}{\partial t'} = g\beta(T' - T'_\infty) - \frac{\sigma B_o^2 u'}{\rho} + \nu \frac{\partial^2 u'}{\partial y'^2} + g\beta^*(C' - C'_\infty) \tag{1}$$

$$\rho c_p \frac{\partial T'}{\partial t'} = k \frac{\partial^2 T'}{\partial y'^2} - Q^*(T' - T'_\infty) - \frac{\partial q_r}{\partial y'} \tag{2}$$

$$\frac{\partial C'}{\partial t'} = D \frac{\partial^2 C'}{\partial y'^2} \tag{3}$$

The boundary conditions are

$$\left.\begin{array}{l} u' = 0,\ T' = T'_\infty,\ C' = C'_\infty \qquad \forall\ y',\ t' \le 0 \\ \left.\begin{array}{l} u' = u_o t' \\ T' = T'_\infty + (T'_w - T_\infty)\frac{u_o^2}{\nu}\ t' \\ C' = C'_\infty + (C'_w - C_\infty)\frac{u_o^2}{\nu}\ t' \end{array}\right\} at\ y' = 0,\ t' > 0 \\ u' \to 0,\ T' \to T'_\infty,\ C' \to C'_\infty\ as\ y' \to \infty,\ t' > 0 \end{array}\right\} \tag{4}$$

The local radiant is expressed as

$$\frac{\partial q_r}{\partial y'} = -4a^*\sigma(T_\infty'^4 - T'^4) \tag{5}$$

where a^* is the absorption constant. Neglecting the higher order terms, T'^4 takes the form as

$$T'^4 \cong 4T_\infty'^3\ T' - 3T_\infty'^4 \tag{6}$$

Introducing non- dimensional quantities:

$$u = \frac{u'}{u_o}, \quad y = \frac{y'}{\nu}u_o, \quad t = \frac{t'u_o^2}{\nu}, \quad H = \frac{Q^*\nu^2}{ku_o^2}, \quad R = \frac{16a^*\sigma\nu^2T_\infty'^3}{ku_o^2}$$

$$\theta = \frac{(T'-T'_\infty)}{(T'_w-T'_\infty)}, \quad C = \frac{(C'-C'_\infty)}{(C'_w-C'_\infty)}, \quad G_r = \frac{\nu g\beta(T'_w-T'_\infty)}{u_o^3}, \quad G_m = \frac{\nu g\beta^*(C'_w-C'_\infty)}{u_o^3} \tag{7}$$

$$M = \frac{\sigma B_o^2\nu}{\rho u_o^2}, \quad P_r = \frac{\nu\rho c_p}{k}, \quad S_c = \frac{\nu}{D}$$

From (5) – (7), equations (1) - (3) with conditions (4) reduce to

$$\frac{\partial u}{\partial t} = \frac{\partial^2 u}{\partial y^2} + G_r\theta + G_mC - Mu \tag{8}$$

$$P_r\frac{\partial\theta}{\partial t} = \frac{\partial^2\theta}{\partial y^2} - (R+H)\theta \tag{9}$$

$$S_c\frac{\partial C}{\partial t} = \frac{\partial^2 C}{\partial y^2} \tag{10}$$

$$\left.\begin{array}{l} u(y,t) = 0, \theta(y,t) = 0, C(y,t) = 0 \qquad \forall \ \ y \text{ and } t \le 0 \\ u(y,t) = t, \theta(y,t) = t, C(y,t) = t \text{ for } y \ = 0 \ and \ \ t > 0 \\ u(y,t) \to 0, \theta(y,t) \to 0, C(y,t) \to 0 \text{ as } y \to \infty \text{ and } t > 0 \end{array}\right] \tag{11}$$

SOLUTION

Equations (8)-(10) with conditions (11) are evaluated by Laplace Transformation method. The results are as:

$$\theta(y,t) = C_3exp(\alpha_4)erfc(\beta_7) + C_4exp(-\alpha_4)erfc(\beta_8)$$

$$C(y,t) = C_5erfc(\beta_{11}) - \alpha_6\exp(-\beta_{11}^2)$$

$$u(y,t) = A_1[C_1exp(\alpha_1)erfc(\beta_1) + C_2exp(-\alpha_1)erfc(\beta_2)] - \frac{A_2}{2}[exp(\alpha_1)erfc(\beta_1) +$$

$$exp(-\alpha_1)erfc(\beta_2)] + \frac{B_3}{2}exp(-\gamma_1)[exp(\alpha_2)erfc(\beta_3) + exp(-\alpha_2)erfc(\beta_4)] +$$

$$\frac{B_1}{2}exp(\gamma_2)[exp(\alpha_3)erfc(\beta_5) + exp(-\alpha_3)erfc(\beta_6)] + \frac{B_3}{2}[exp(\alpha_4)erfc(\beta_7) +$$

$$exp(-\alpha_4)erfc(\beta_8)] - \frac{B_3}{2}exp(-\gamma_1)[exp(\alpha_5)erfc(\beta_9) + exp(-\alpha_5)erfc(\beta_{10})] - B_1erfc(\beta_{11}) -$$

$$B_4[C_3exp(\alpha_4)erfc(\beta_7) + C_4exp(-\alpha_4)erfc(\beta_8)] - \frac{B_1}{2}exp(\gamma_2)[exp(\alpha_7)erfc(\beta_{12}) +$$

$exp(-\alpha_7)erfc(\beta_{13})] - B_2[C_5 erfc(\beta_{11}) - \alpha_6 \exp(-\beta_{11}^2)]$

(12)

Nusselt Number

$$N_u = -\left(\frac{\partial\theta(y,t)}{\partial t}\right)_{y=0}$$

$$= (t\sqrt{K} + \frac{P_r}{2\sqrt{K}})\, erf\sqrt{\frac{K}{P_r}t} + \sqrt{\frac{tP_r}{\pi}}\, e^{-\frac{K}{P_r}t}. \quad (13)$$

Sherwood Number

$$S_h = -\left(\frac{\partial C(y,t)}{\partial t}\right)_{y=0} = 2\sqrt{\frac{tS_c}{\pi}}. \quad (14)$$

Skin Friction

$$\tau = -\left(\frac{\partial u(y,t)}{\partial t}\right)_{y=0}$$

$$= U_1\left[\left(t\sqrt{M} + \frac{1}{2\sqrt{M}}\right) erf\sqrt{Mt} + \sqrt{\frac{t}{\pi}}e^{-Mt}\right] - U_2\sqrt{M}erf\sqrt{Mt} + B_3 e^{-lt}\left[\sqrt{M-l}\, erf\sqrt{(M-l)t} - \sqrt{K - lP_r}erf\sqrt{\left(\frac{K}{P_r} - l\right)t}\right] + B_1 e^{nt}\left[\sqrt{M+n}\, erf\sqrt{(M+n)t} - \sqrt{nS_c}erf\sqrt{nt}\right] + \left[(B_3 - tB_4)\sqrt{K} - B_4\frac{P_r}{2\sqrt{K}}\right] erf\sqrt{\frac{K}{P_r}t} - tB_4\sqrt{\frac{P_r}{\pi t}}e^{-\frac{K}{P_r}t} + 2B_2 t\sqrt{\frac{S_c}{\pi t}}. \quad (15)$$

RESULTS AND DISCUSSION

Numerical computations are used to validate the outcome of numerous parameters on the kind of flow to comprehend the physical meaning of the problem. Figures (1) - (12) and Tables (1) - (3) show the numerical data graphically.

Concentration profile for variations in Sc is revealed in Figure. 1. The graph shows that as the Schmidt number rises, plate concentration decreases. Near the wall, there is also an inverse trend.

Figure. 2 shows the concentration profile throughout time. When the duration is increased, the concentration of the plate increases, as shown in the graph.

Figure. 3 depicts the temperature variations as a function of the H and R. The graph portrays that as the H or R is increased, the temperature drops. Using Pr 0.21, 0.71, and 7 as values for Prandtl number, the influence of Pr on temperature is demonstrated. H=2 is used as the heat source/sink parameter, while t = 0.2 is used as the time. The graph indicates reduction in temperature with Pr augment. It's also worth noting that the temperature of water (Pr=7) is lower than that of air (Pr=0.71). Figure.5 depicts the effect of Magnetic field parameter and Prandtl Number on velocity Profile. The fluid flow is demonstrated to be accelerated by a transverse magnetic field. Also fluid slow down with increment in Pr. Variations of Sc on velocity are presented by Figure. 6. The graph displays that velocity decreases with increment in Sc. Figure. 7 depicts the effects Gr and Gm on the velocity. With rising values of the thermal Gr, the velocity climbs slightly near the wall. The graph also indicates that when the mass Grashof number increases, velocity drops.

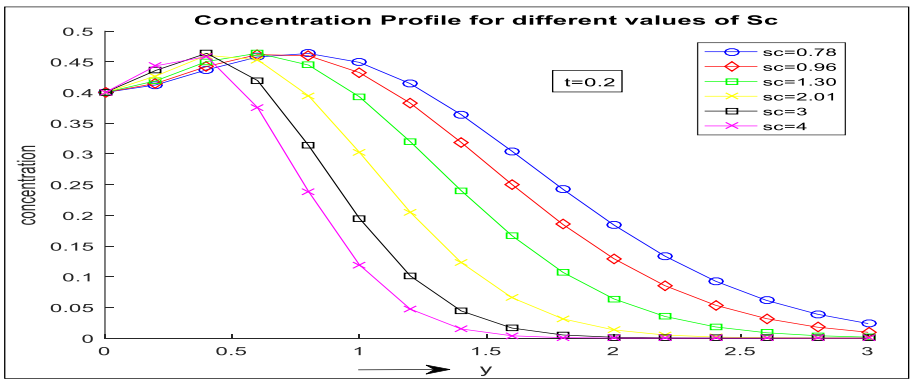

Figure 1. Variations in Concentration at Sc

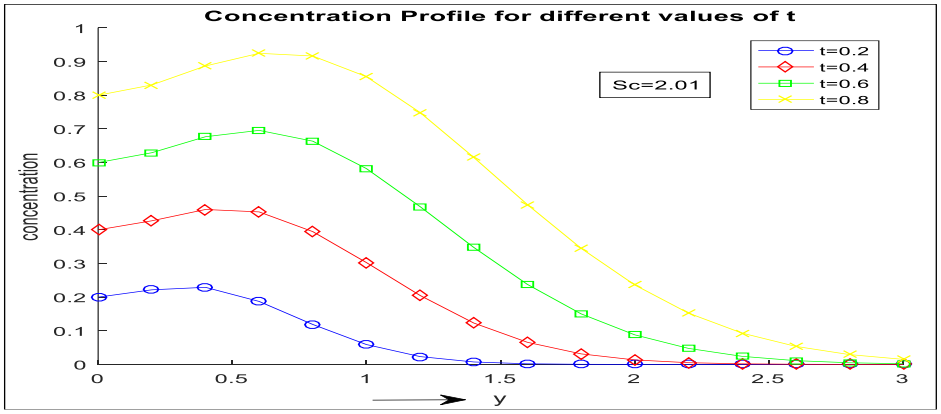

Figure 2. Variations in Concentration at t

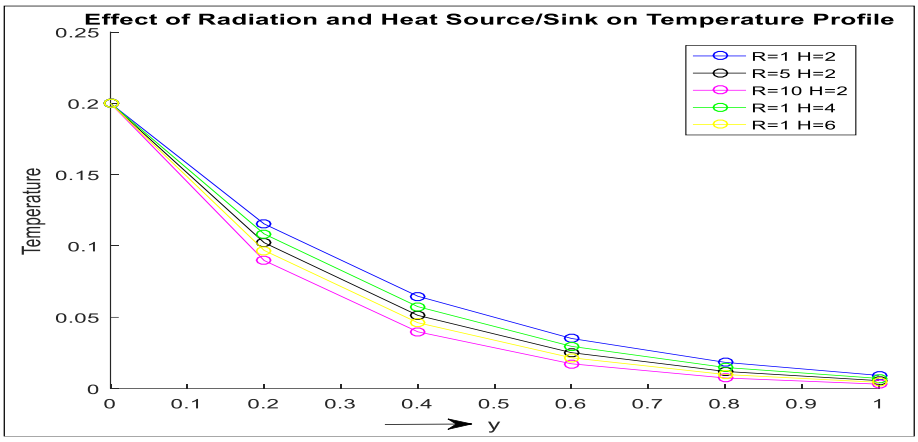

Figure 3. Temperature Variations at H and R

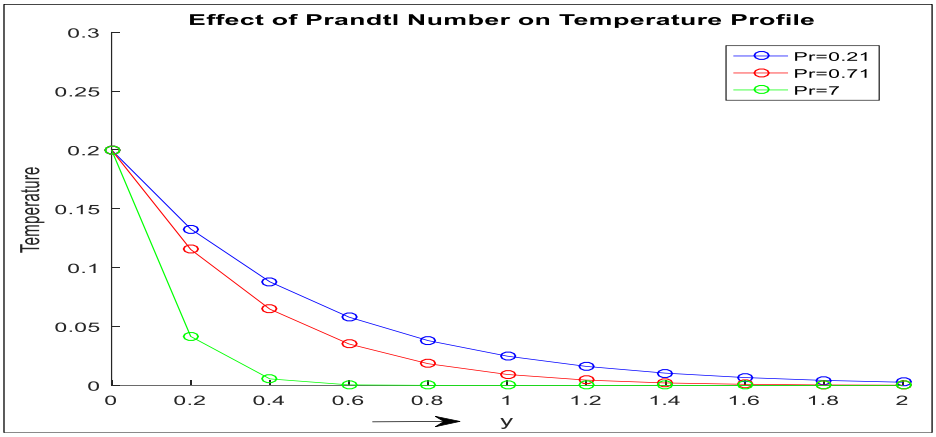

Figure 4. Temperature Variations at t

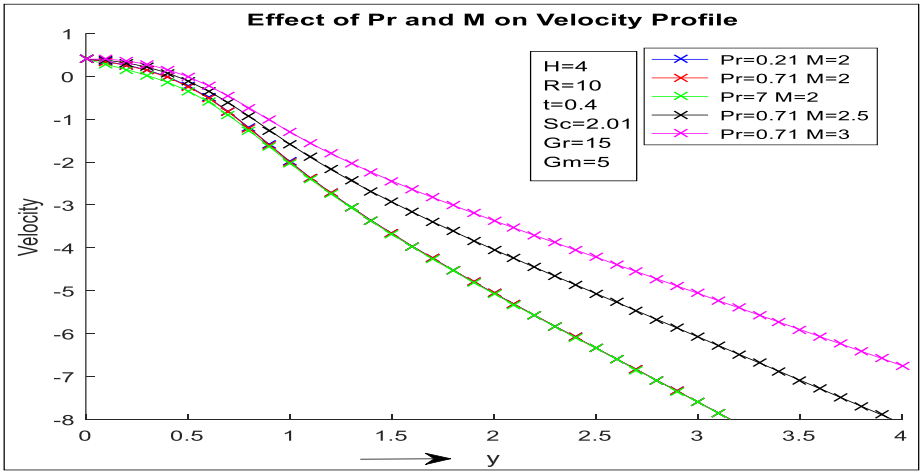

Figure 5. Velocity variations at different Pr and M

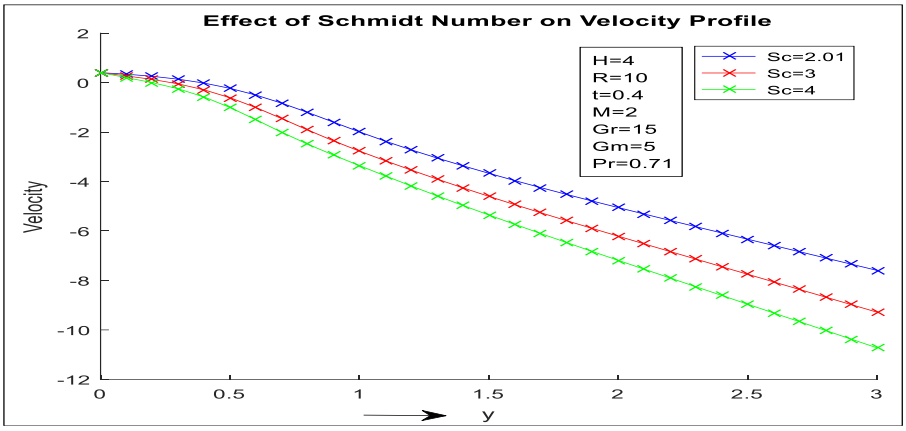

Figure 6. Velocity variations at different Sc

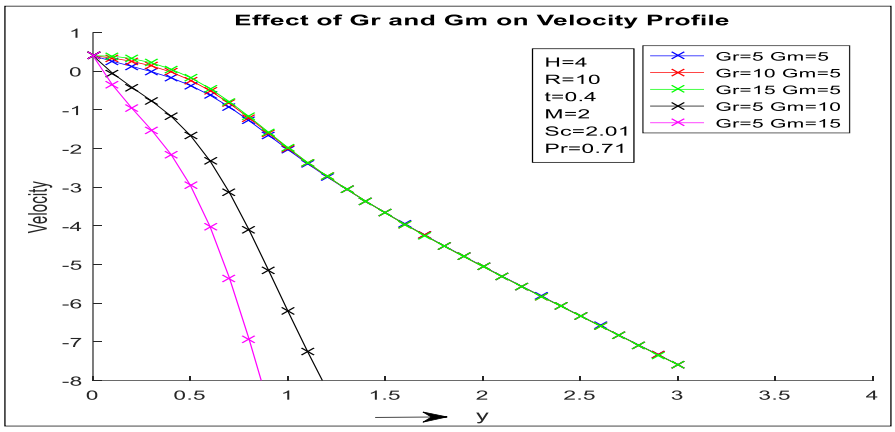

Figure 7. Velocity variations for Gr and Gm

Table 1 shows the variations of Nu. By raising the values of time, heat source parameter, Radiation Parameter and Prandtl Number, the heat transfer rate increases. Figure. 8 depicts these impacts graphically.

Table 1. Nusselt Number Variations

t	H	R	Pr	Nu
0.2	2	10	0.71	0.7951
0.4	2	10	0.71	1.4881
0.6	2	10	0.71	2.1809
0.2	4	10	0.71	08431
0.2	6	10	0.71	0.8887
0.2	2	15	0.71	0.9107
0.2	2	20	0.71	1.0138
0.2	2	10	0.21	0.7231
0.2	2	10	0.16	0.7159

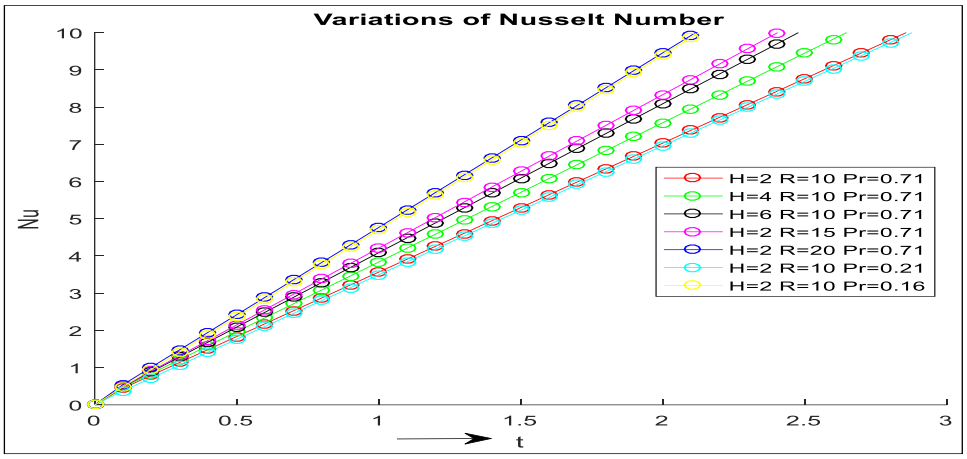

Figure 8. Variations of Nusselt Number at H, R and Pr

Table 2 and Figure 9 exhibit Sherwood number variations. Sherwood number increases with Schmidt number and time, as shown in the graph. Table 3 and Figures. 10 and 11 demonstrate differences in skin friction at various values. As t, H, R, M, Sc, and Pr increase, skin friction also increases. Increment in Gr and Gm also indicates a reduction in the value of skin friction.

Table 2. Sherwood Number Variations

Time(t)/Sc → ↓	0.63	0.78	2.01	3	4
0.1	0.2832	0.3151	0.5059	0.6180	0.7136
0.2	0.4005	0.4457	0.7154	0.8740	1.0093
0.3	0.4906	0.5458	0.8762	1.0705	1.2361
0.4	0.5664	0.6303	1.0118	1.2361	1.4273
0.5	0.6333	0.7047	1.1312	1.3820	1.5958
0.6	0.6937	0.7719	1.2392	1.5139	1.7481
0.7	0.7493	0.8338	1.3384	1.6352	1.8881
0.8	0.8011	0.8913	1.4309	1.7481	2.0185
0.9	0.8497	0.9454	1.5177	1.8541	2.1409
1	0.8956	0.9966	1.5998	1.9544	2.2568

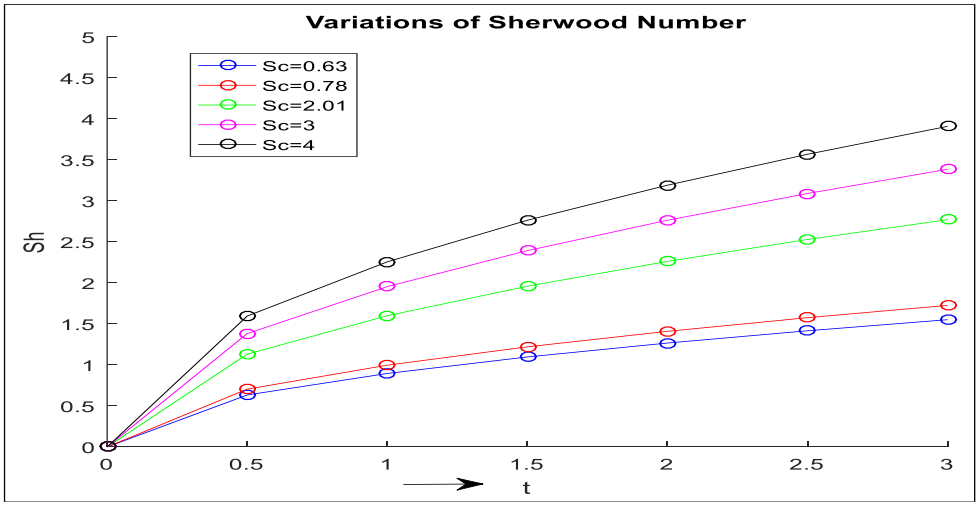

Figure 9. Variations of Sherwood Number

Table 3. Skin Friction Variations

(t)	(H)	(R)	(M)	(Sc)	(Gr)	(Gm)	(Pr)	(τ)
0.2	**4**	**10**	**1**	**2.01**	**1**	**1**	**0.71**	0.4828
0.3	4	10	1	2.01	1	1	0.71	0.5825
0.4	4	10	1	2.01	1	1	0.71	0.6641
0.2	**8**	10	1	2.01	1	1	0.71	0.4842
0.2	**10**	10	1	2.01	1	1	0.71	0.4849
0.2	4	**15**	1	2.01	1	1	0.71	0.4846
0.2	4	**20**	1	2.01	1	1	0.71	0.4860
0.2	4	10	**1.5**	2.01	1	1	**0.71**	0.4993
0.2	4	10	**2**	2.01	1	1	**0.71**	0.5155
0.2	4	10	1	**3**	1	1	0.71	0.4859
0.2	4	10	1	**4**	1	1	0.71	0.4881
0.2	4	10	1	2.01	**2**	1	0.71	0.4554
0.2	4	10	1	2.01	**3**	1	0.71	0.4280
0.2	4	10	1	2.01	1	**2**	0.71	0.4554
0.2	4	10	1	2.01	1	**3**	0.71	0.4280
0.2	4	10	1	2.01	1	1	**0.21**	0.4809
0.2	4	10	1	2.01	1	1	**0.16**	0.4807

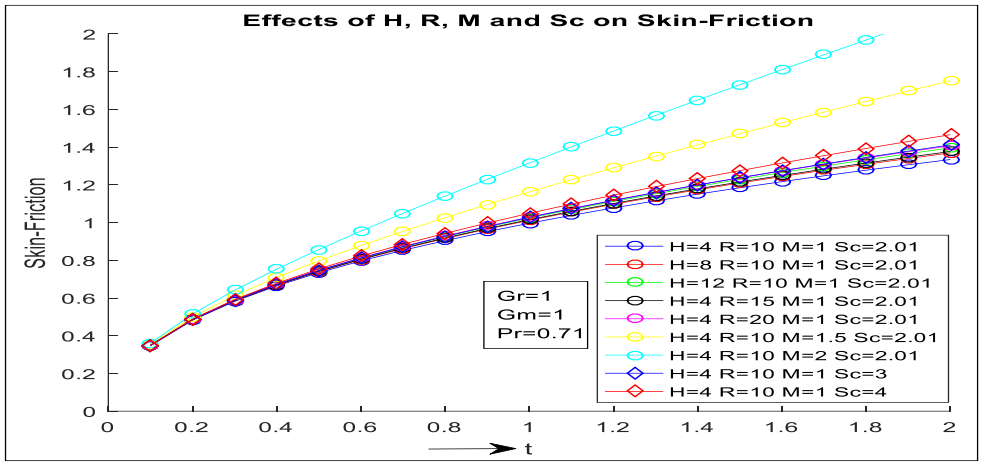

Figure 10. Skin-Friction Variations at different H, R, M and Sc

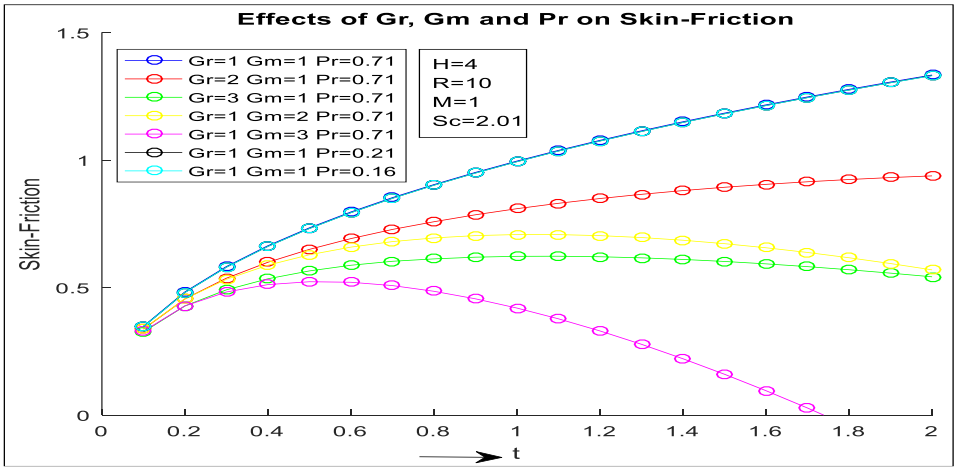

Figure 11. Skin-Friction Variations at different Gr, Gm and Pr

(Garg et al., 2011) studied the same problem with radiation effects instead of effects of heat source/ sink. Also results can be compared with (Garg and Shipra, 2019) taking R=0. It is noticed that results of temperature, concentration, Nusselt number are exactly same but results of velocity, skin-friction and Sherwood number are slightly different at some parameters. Skin-Friction also shows opposite results on Heat Source/sink parameter.

CONCLUSIONS

The study can be concluded as:

(i) Concentration of a species grows as time passes, whereas mass diffusivity reduces it.

(ii) The temperature of the fluid is reduced with enhancement in viscosity, radiation, and heat absorption parameter.

(iii) The fluid motion is accelerated by magnetic field and thermal buoyancy forces, but augmentation in mass diffusivity, viscosity, buoyancy forces show reverse trend of fluid motion.

(iv) With escalation in time, viscosity, heat source parameter and radiation parameter, the heat transfer rate increases.

(v) Mass transfer rate increases with development of time whereas a reverse trend is noted with expansion in mass diffusivity.

(vi) Time, heat absorption parameter, mass diffusivity enhance shear stress whereas buoyancy forces diminish it.

APPENDIX

$K = R + H,\ \ n = \frac{M}{S_c - 1}\ ,\ \ l = \frac{K - M}{P_r - 1},\ U = 1 - B_2 + B_4\ ,\ \ U_2 = \ B_1 + \ B_3,\ \gamma_1 = lt,\ \ \gamma_2 = nt,$

$B_1 = \frac{G_m(S_c - 1)}{M^2}\ ,\ \ B_2 = \frac{G_m}{M},\ \ B_3 = \frac{G_m(P_r - 1)}{(K - M)^2},\qquad B_4 = \frac{bG_m - G_r}{H - M}$

$C_1 = \frac{t}{2} + \frac{y}{4\sqrt{M}},\quad C_2 = \frac{t}{2} - \frac{y}{4\sqrt{M}}\ ,\ \ C_3 = \frac{t}{2} + \frac{y}{4\sqrt{K}}P_r,\ \ C_4 = \frac{t}{2} - \frac{y}{4\sqrt{K}}P_r,\ \ C_5 = t + \frac{y^2}{2}S_c\ ,$

$\alpha_1 = y\sqrt{M},\ \ \alpha_2 = y\sqrt{M - l},\quad \alpha_3 = y\sqrt{M + n}\ ,\ \ \alpha_4 = y\sqrt{K},\qquad \alpha_5 = y\sqrt{K - lP_r},$

$\alpha_6 = y\sqrt{\frac{tS_c}{\pi}}\ ,\ \ \alpha_7 = y\sqrt{nS_c},\ \ \beta_1 = \frac{y}{2\sqrt{t}} + \sqrt{Mt}\ ,\qquad \beta_2 = \frac{y}{2\sqrt{t}} - \sqrt{Mt}\ ,$

$\beta_3 = \frac{y}{2\sqrt{t}} + \sqrt{(M - l)t}\ ,\ \ \beta_4 = \frac{y}{2\sqrt{t}} - \sqrt{(M - l)t},\qquad \beta_5 = \frac{y}{2\sqrt{t}} + \sqrt{(M + n)t}\ ,$

$\beta_6 = \frac{y}{2\sqrt{t}} - \sqrt{(M + n)t},\ \beta_7 = \frac{y}{2\sqrt{t}}\sqrt{P_r} + \sqrt{\frac{K}{P_r}t}\ ,\qquad \beta_8 = \frac{y}{2\sqrt{t}}\sqrt{P_r} - \sqrt{\frac{K}{P_r}t}\ ,$

$$\beta_9 = \frac{y}{2\sqrt{t}}\sqrt{P_r} + \sqrt{\left(\frac{K}{P_r} - l\right)t}\ , \quad \beta_{10} = \frac{y}{2\sqrt{t}}\sqrt{P_r} - \sqrt{\left(\frac{K}{P_r} - l\right)t}$$

$$\beta_{11} = \frac{y}{2\sqrt{t}}\sqrt{S_c}\ , \ \beta_{12} = \frac{y}{2\sqrt{t}}\sqrt{S_c} + \sqrt{nt}\ , \qquad \beta_{13} = \frac{y}{2\sqrt{t}}\sqrt{S_c} - \sqrt{nt}$$

NOMENCLATURE

a	accelerated parameter	Q^*	coefficient of Heat Source/Sink
B_o	electromagnetic induction	Sc	Schmidt number
C'	species concentration	Sh	Sherwood number
C'_w	species concentration near the wall	t'	time
C'_∞	species concentration far away wall	t	dimensionless time
	the wall	T'	Fluid temperature
Cp	specific heat at constant pressure	T'_w	Fluid temperature near the wall
D	chemical molecular diffusivity	T'_∞	Fluid temperature far away the wall
D_l	coefficient of thermal diffusivity	u'	velocity in x'-direction
erf	Error Function	u	dimensionless velocity
erfc	Complementary Error Function		**Greek Symbols**
g	acceleration due to Gravity	σ	electrical conductivity of the fluid
Gm	Mass Grashof number	β	coefficient of volume expansion
Gr	Thermal Grashof number	β^*	coefficient of thermal expansion
H	Heat source/sink parameter	ρ	density
K	Chemical reaction parameter	k	thermal conductivity
K_l	reaction rate constant	ν	kinematic viscosity
M	Magnetic field parameter	θ	dimensionless temperature
MHD	Magnetohydrodynamics	τ	dimensionless skin-friction
Nu	Nusselt number		

REFERENCES

Abdelrazik, A. S., Tan, K. H., Aslfattahi, N., Arifutzzaman, A., Saidur, R., & Al-Sulaiman, F. A. 2020. Optical, stability and energy performance of water-based MXene nanofluids in hybrid PV/thermal solar systems. Solar Energy. **204**: 32-47.

Afzal, A., Yashawantha, K.M., Aslfattahi, N., Saidur, R., Abdul Razak, R.K. and Subbiah, R. 2021. Back propagation modeling of shear stress and viscosity of aqueous Ionic-MXene nanofluids. Journal of Thermal Analysis and Calorimetry. **145(4)**: 2129-2149.

Basant, K.J. and Gabriel, S. 2020. Effect of heat source/sink on MHD free convective flow in a channel filled with nanofluid in the existence of induced magnetic field: an analytic. SN Applied Sciences. **2**: 1321.

Das, U.N., Ray, S.N. and Soundalgekar, V.M. 1996. Mass transfer effects on flow past an impulsively started infinite vertical plate with constant mass flux—an exact solution. Heat and Mass transfer. **31(3)**: 163-167.

England, W.G. and Emery, A.F. 1969. Thermal radiation effects on the laminar free convection boundary layer of an absorbing gas.

Garg, B. P. & Shipra. **2019.** Heat source/sink effect on MHD free convective mass transfer flow flow past an accelerated vertical plate. I-Manager's Journal on Future Engineering and Technology. **14 (3)**: 35-42.

Garg, B. P., Singh, K. D. & Bansal, N. 2015. Injection\Suction effect on spanwise sinusoidal fluctuating MHD mixed convection flow through porous medium in a vertical porous channel with thermal radiation. Journal Rajasthan Academy Physical Sciences. **14**: 73-88.

Garg, B. P., Singh, K. D. & Pathak, R. 2011. An analysis of radiative, free-convective and mass transfer flow for an accelerated vertical plate in presence of transverse magnetic field. Journal Rajasthan Academy Physical Sciences. **10(1)**: 1-10.

Hossain, M.A. & Takhar, H.S. 1996. Radiation effect on mixed convection along a vertical plate with uniform surface temperature. Heat and Mass transfer. **31(4)**: 243-248.

Kandasamy, R., Periasamy, K. & Prabhu, K.S. 2005. Chemical reaction, heat and mass transfer on MHD flow over a vertical stretching surface with heat source and thermal stratification effects. International Journal of Heat and Mass Transfer. **48(21-22)**: 4557-4561.

Kumar, K. G., Reddy, M. G., Sudharani, M. V. V. N. L., Shehzad, S. A., & Chamkha, A. J. 2020. Cattaneo–Christov heat diffusion phenomenon in Reiner–Philippoff fluid through a transverse magnetic field. Physica A: Statistical Mechanics and Its Applications. **541**: 123330.

Rajput, U.S. & Sahu, P.K. 2011. Transient free convection MHD flow between two long vertical parallel plates with constant temperature and variable mass diffusion. Journal of Math. Analysis **34(5)**:1665-1671.

Soundalgekar, V.M., Patil, M.R. & Jahagirdar, M.D. 1981. MHD Stokes problem for a vertical infinite plate with variable temperature. Nuclear Engineering and design. **64(1)**: 39-42.

Wakif, A., Chamkha, A., Animasaun, I. L., Zaydan, M., Waqas, H., & Sehaqui, R. 2020. Novel physical insights into the thermodynamic irreversibilities within dissipative EMHD fluid flows past over a moving horizontal riga plate in the coexistence of wall suction and joule heating effects: a comprehensive numerical investigation. Arabian Journal for Science and Engineering. **45(11)**: 9423-9438.